JOC The Journal of Organic Chemistry

Article

pubs.acs.org/joc

Mechanistic Study on Gold-Catalyzed Highly Selective Hydroamination of Alkylidenecyclopropanes

Chen Wang,[†] Xiao-Rong Ren,[†] Chen-Ze Qi,*[,†] and Hai-Zhu Yu*[,‡]

[†]Zhejiang Key Laboratory of Alternative Technologies for Fine Chemicals Process, Shaoxing University, Shaoxing 312000, China

[‡]Department of Chemistry and Center for Atomic Engineering of Advanced Materials, Anhui University, Hefei 230601, China

Supporting Information

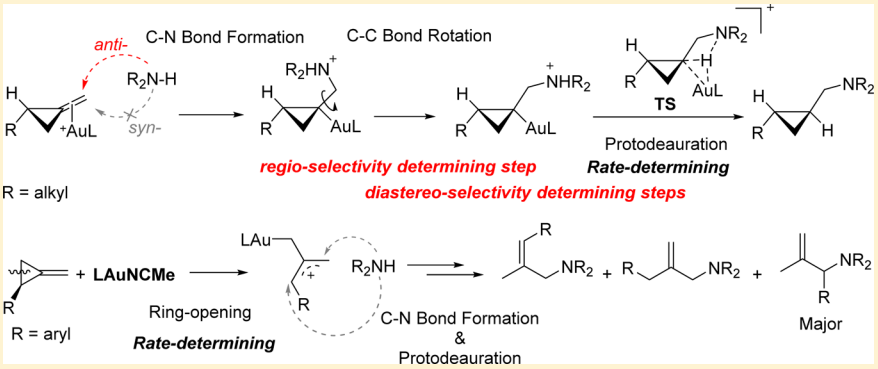

ABSTRACT: Density functional theory calculations have been carried out to study the mechanism of the gold-catalyzed highly selective hydroamination of alkylidenecyclopropanes. Two main mechanisms (i.e., double-bond activation-first and three-membered-ring activation-first mechanisms) have been examined. The double-bond activation-first mechanism results in the alkene hydroamination product, and it mainly consists of three steps: C−N bond formation, C−C bond rotation, and protodeauration (rate-determining step). Meanwhile, the three-membered-ring activation-first mechanism finally produces allylic amines, and it occurs via the ring-opening (rate-determining step), C−N bond formation, and protodeauration steps. The calculation results show good agreement with the experimental outcomes on the chemo-, regio-, and diastereoselectivity. On this basis, we found that the regioselectivity is caused by the C−C bond rotation step, while the diastereoselectivity is determined by both the C−C bond rotation and the protodeauration steps in the double-bond activation-first mechanism.

INTRODUCTION

Transition-metal-catalyzed functionalization of unsaturated hydrocarbons has become a powerful strategy in constructing structurally complex molecules.[1] In particular, hydroamination of alkenes has attracted increasing interest in recent decades due to its great potential in synthesizing natural products and drugs.[2] To date, numerous transition-metal catalysts (including Rh, Ru, Pd, Pt, Cu, Au, etc.) have been developed to promote the hydroamination of alkenes.[2a] Herein, it is interesting to note that for most of the previously reported hydroamination reactions of terminal alkenes the Markovnikov products are favorably generated,[3] whereas the *anti*-Markovnikov hydroamination is challenging and rarely reported.[4] Specifically, Widenhoefer and co-workers reported the gold-catalyzed hydroamination of alkylidenecyclopropanes (ACPs) with imidazolidin-2-ones (Scheme 1)[5] in which the *anti*-Markovnikov hydroamination products (rather than the Markovnikov hydroamination products) are exclusively formed. Their study provides the first example for the gold-catalyzed *anti*-Markovnikov hydroamination of the alkenes. Another significant feature of this reaction is the chemoselectivity. In previous studies on transition-metal-catalyzed reactions of ACPs, the ring-opened products were preferentially formed due to the high ring strain.[6] By contrast, in Widenhoefer's study, the alkene hydroamination products were predominantly formed over the ring-opened products. Furthermore, the diastereose-

Scheme 1. Gold-Catalyzed Anti-Markovnikov Hydroamination of Alkylidenecyclopropanes

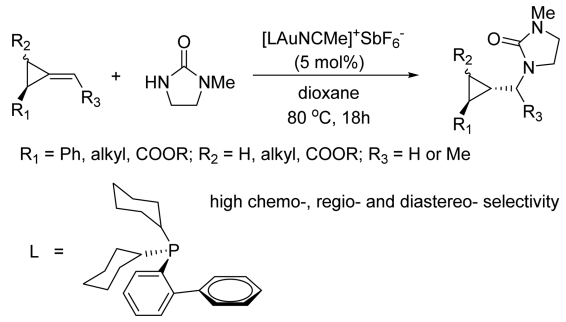

Received: April 5, 2016
Published: July 22, 2016

DOI: 10.1021/acs.joc.6b00726
J. Org. Chem. 2016, 81, 7326−7335

Scheme 2. Model Reaction Used in Our Theoretical Studies

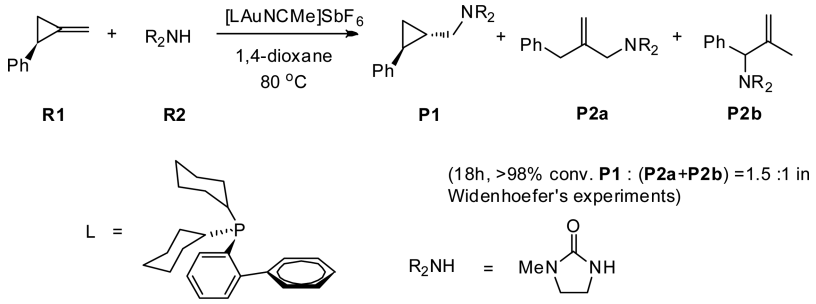

lectivity of the reaction (*anti*-hydroamination over the *syn*-products) is also highly attractive.

On the basis of the NMR spectroscopic analysis and control experiments, Widenhoefer and co-workers suggested that the mechanistic origin of the regioselectivity might relate to the partial sp hybridization character of the internal alkene carbon atom (connecting the ACP group). Widenhoefer's study provided fundamental insights into the regioselectivity.[5] Nevertheless, the current mechanistic understanding on this reaction remains quite limited. First, the reason for the favorable activation of the double bond (compared to the three-membered ring) in ACP is still unknown.[7] According to the recent theoretical studies,[8,9] either the double bond or the three-membered ring can be effectively activated by the Au(I) catalyst. Second, the details of the nucleophilic attack (such as the attacking site/direction) and the proton-transfer (the most feasible proton transfer mode) steps need to be clarified. Third, all the C−C bonds in the three-membered ring are labile and might possibly dissociate, and the relative activities of them are currently unknown. In other words, the detailed information for each step of the overall mechanism, the rate-determining step, and especially the origin of the high chemo-, regio-, and diastereoselectivity deserve further investigation. To settle these issues, we carried out a systemic mechanistic study on Au(I)-catalyzed hydroamination of alkylidenecyclopropane with 1-methylimidazolidin-2-one with the density functional theory (DFT) methods.

COMPUTATIONAL DETAILS

Methods. All calculations were performed with the Gaussian 09 package.[10] The solution-phase geometry optimizations were carried out using the B3LYP functional[11] with a combined basis set BSI (i.e., Lanl2DZ for Au, Sb and 6-31G(d) for the other atoms). Corresponding to the experimental conditions,[5] 1,4-dioxane is used as the solvent (with SMD model),[12] and the temperature is set as 353.15 K. Frequency calculations were performed (with the same method as optimization) to confirm each stationary point to be either a local minimum (0 imaginary frequency) or a transition state (1 imaginary frequency). For each transition state, intrinsic reaction coordinate (IRC) analysis[13] was used to ensure that it connects the right reactant and product. On the basis of the optimized geometries, M06-L functional[14] with the BSII basis set (i.e., CEP-121G with an additional f-polarization function for Au, CEP-121G for Sb and 6-311++G(2df,2p) for the other atoms) was used to calculate the single-point energies of all species in 1,4-dioxane solvent (with an SMD solvation model).

Since DFT calculations are known to overestimate the entropic effect (especially when the number of reactants and products are unequal),[15] the single-point energies corrected by the enthalpy thermal corrections were used to describe all of the energies throughout this study. Note that in previous studies[16] total electronic energies with the zero-point energy corrections were also used to evaluate the energetics. For our system, the conclusions made from the energies with zero-point energy correction are consistent with those from the relative enthalpies (see the Supporting Information for more details). 3D structures were illustrated using CYLview.

Model Reaction. The reaction of (*S*)-1-phenyl-2-methylenecyclopropane (**R1**) with 1-methyl-imidazolidin-2-one (**R2**) catalyzed by [{PCy_2(*o*-biphenyl)}Au(NCMe)]$^+SbF_6^-$ (PCy_2(*o*-biphenyl) was denoted as **L**) was chosen as a model reaction (Scheme 2). This reaction yields the *anti*-Markovnikov hydroamination product (**P1**) and the allylic amines (**P2a** and **P2b**) in a ratio of 1.5:1.

In the model system, the Au(I) center might possibly coordinate with different species, including NCMe, the substrates (**R1** and **R2**), and the solvent (1,4-dioxane). Therefore, we first evaluated the relative stabilities of the different complexes (Scheme 3). According to the calculation results, the most stable Au(I) complex is **LAuNCMe**. Therefore, the enthalpies of **LAuNCMe**, **R1**, and **R2** are set as the energetic reference in this study.

Scheme 3. Relative Stabilities of Different Au(I) Complexes

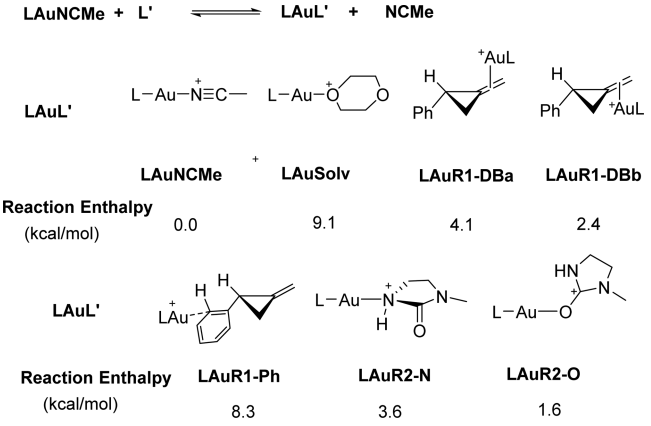

RESULTS

As mentioned in the Introduction, the reaction might start with the activation of either the double bond or the three-membered ring of **R1**. Meanwhile, starting from the structure of the amide-ligated Au(I) complex **LAuR2-N**, it is also possible that the reaction begins with the N−H bond dissociation of the amide substrate.[17] For clarity reasons, these pathways are named as double-bond activation-first, three-membered-ring activation-first, and amide activation-first mechanisms, respectively. For clarity reasons, an illustrative diagram for these pathways is given in Scheme 4.

Amide Activation-First Mechanism. The possibility of activating the N−H bond with an external proton acceptor (MeCN, 1,4-dioxane, SbF_6^-, or **R2**) was first examined. The acid−base reactions of them with **LAuR2-N** are all highly endothermic (>30 kcal/mol), indicating that the activation of

DOI: 10.1021/acs.joc.6b00726
J. Org. Chem. 2016, 81, 7326−7335

Scheme 4. Main Mechanistic Possibilities Examined in This Study

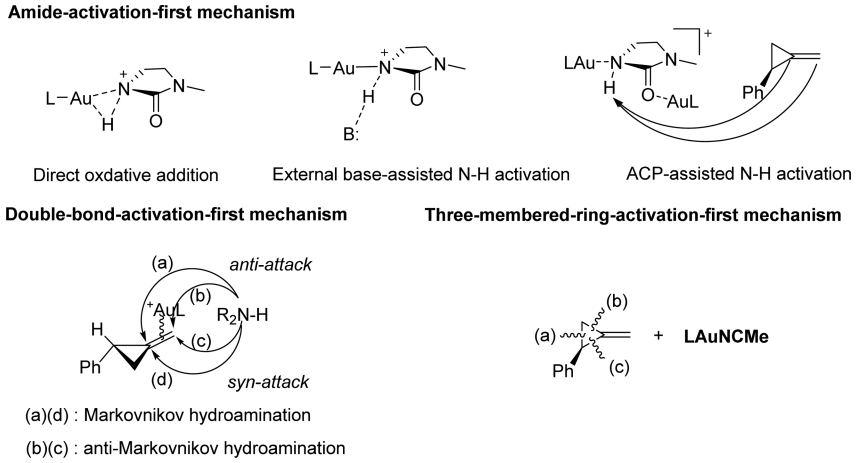

Scheme 5. Possible N−H Bond Activation Modes[a]

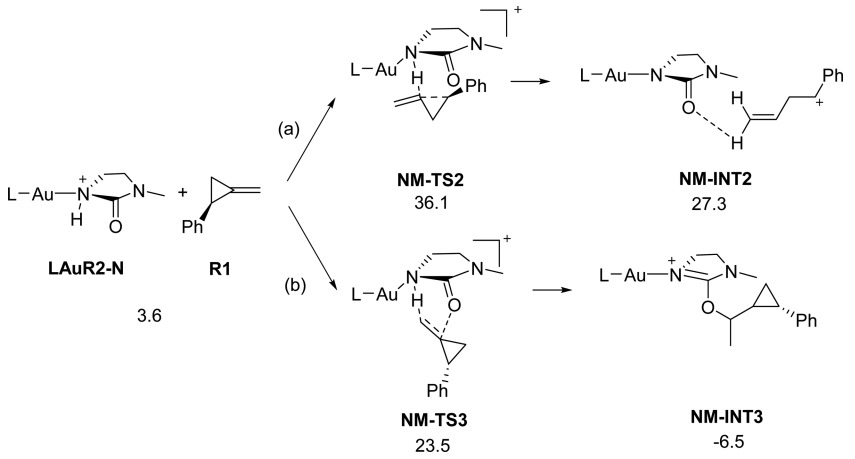

[a]Enthalpies are in kcal/mol.

the N−H bond by an external base is unlikely (Scheme S2). Meanwhile, we also considered the possibility of the three-membered-ring or double-bond-mediated N−H activation mechanism on **LAuR2-N** (Scheme 5). In the former case, the internal carbon of the double bond (C2) accepts the proton, and the three-membered ring is broken to form a benzyl carbocation (Scheme 5a). The activation enthalpy for this process is 36.1 kcal/mol (**NM-TS2**), and the relative enthalpy of the formed intermediate **NM-INT2** is 27.3 kcal/mol. In the latter case, the activation enthalpy for the proton transfer to the terminal carbon of the double bond (C1) is 23.5 kcal/mol (**NM-TS3**), and the relative enthalpy of the formed **NM-INT3** is −6.5 kcal/mol (Scheme 5b).

Note that some other N−H activation mechanisms (such as the N−H oxidative addition and ACP mediated N−H activation on **LAuR2-O**) were also examined but excluded due to their high enthalpy demands (Schemes S1 and S3). According to the aforementioned results and discussions, the double-bond-mediated pathway (Scheme 5b) represents the most favorable N−H activation pathway. The overall activation barrier is 23.5 kcal/mol, and the relative enthalpy of the formed intermediate **NM-INT3** is −6.5 kcal/mol.

Double-Bond Activation-First Mechanism. The double-bond activation-first mechanism starts from the coordination of the double bond to the gold atom (Scheme 3, **LAuR1-DBa** or **LAuR1-DBb**; note that the difference between **LAuR1-DBa** and **LAuR1-DBb** lies in the position of the Au complexes relative to the Ph substituent). Then, the attack of the N atom of **R2** to the internal or terminal carbon of the double bond will finally produce the Markovnikov and *anti*-Markovnikov products, respectively.

For the Markovnikov addition, the N atom may attack the internal carbon of the double bond from either the *syn*- or the *anti*- position with respect to the phenyl group (Scheme 6). Starting from **LAuR1-DBa**, the *syn*-attack (Scheme 6a) generates the intermediate **DM-INT1a** with an enthalpy barrier of 10.6 kcal/mol (**DM-TS1a** relative to **LAuR1-DBa** and **R2**). After that, the proton transfer from the N atom to the terminal carbon and the simultaneous C−Au bond cleavage (proto-deauration) will lead to the formation of the *syn*-Markovnikov hydroamination product. Finally, the catalyst is regenerated after the coordination of MeCN to the Au(I). In all, the possibility for this pathway could be excluded due to the high enthalpy of the transition state **DM-TS2a**.

Starting from **LAuR1-DBa**, the *anti*-attack of the N atom to the internal carbon of the double bond occurs via the transition state **DM-TS1b**, and the enthalpy barrier is 14.4 kcal/mol (**DM-TS1b** relative to **LAuR1-DBb** and **R2**, Scheme 6b). Thereafter, the formed **DM-INT1b** undergoes a facile protodeauration process to form the *anti*-Markovnikov hydro-

DOI: 10.1021/acs.joc.6b00726
J. Org. Chem. 2016, 81, 7326−7335

Scheme 6. Markovnikov Hydroamination of the Double Bond Starting from LAuR1-DBa[a]

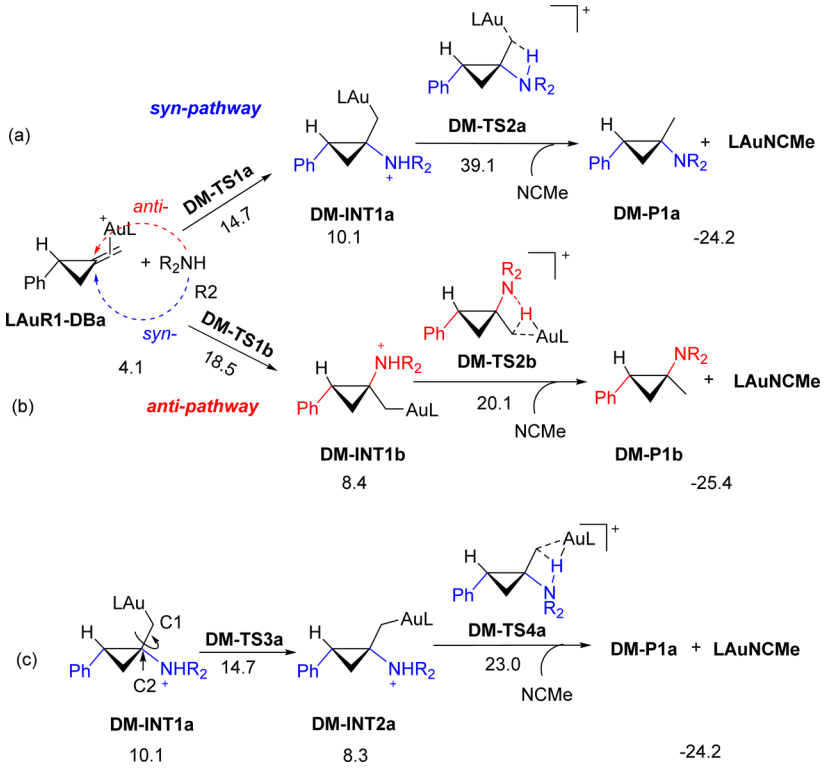

[a]Enthalpies are in kcal/mol.

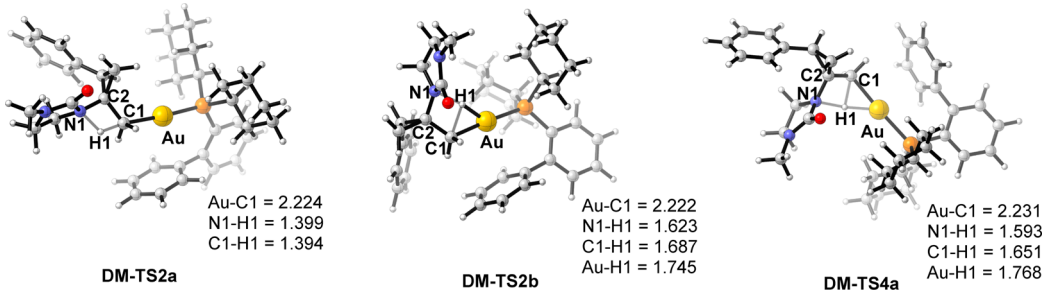

Figure 1. Optimized structures of **DM-TS2a** and **DM-TS2b**. Bond distances are in angstroms.

Scheme 7. Markovnikov Hydroamination of the Double Bond Starting from LAuR1-DBb[a]

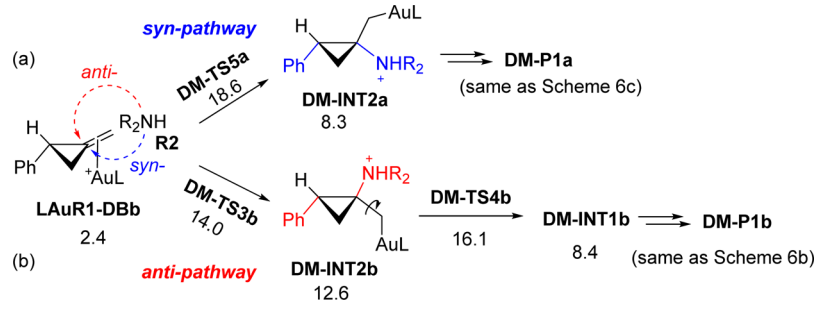

[a]Enthalpies are in kcal/mol.

amination product (**DM-INT1b** → **DM-TS2b** → **DM-P1b**). The enthalpy of **DM-TS2b** is only 20.1 kcal/mol, significantly lower than that of **DM-TS2a** in Scheme 6a. Comparing the optimized structures of these two transition states (Figure 1), we found that the agostic interaction between Au and the H atom might contribute to the extra stability of **DM-TS2b**. Inspired by this observation, we proposed another mechanistic possibility. As shown in Scheme 6c, **DM-INT1a** can easily isomerize to another configuration by rotating the C1−C2 bond (**DM-INT1a** → **DM-TS3a** → **DM-INT2a**) and then undergoes the Au-assisted protodeauration process via **DM-**

DOI: 10.1021/acs.joc.6b00726
J. Org. Chem. 2016, 81, 7326−7335

Scheme 8. *anti*-Markovnikov Hydroamination of the Double Bond[a]

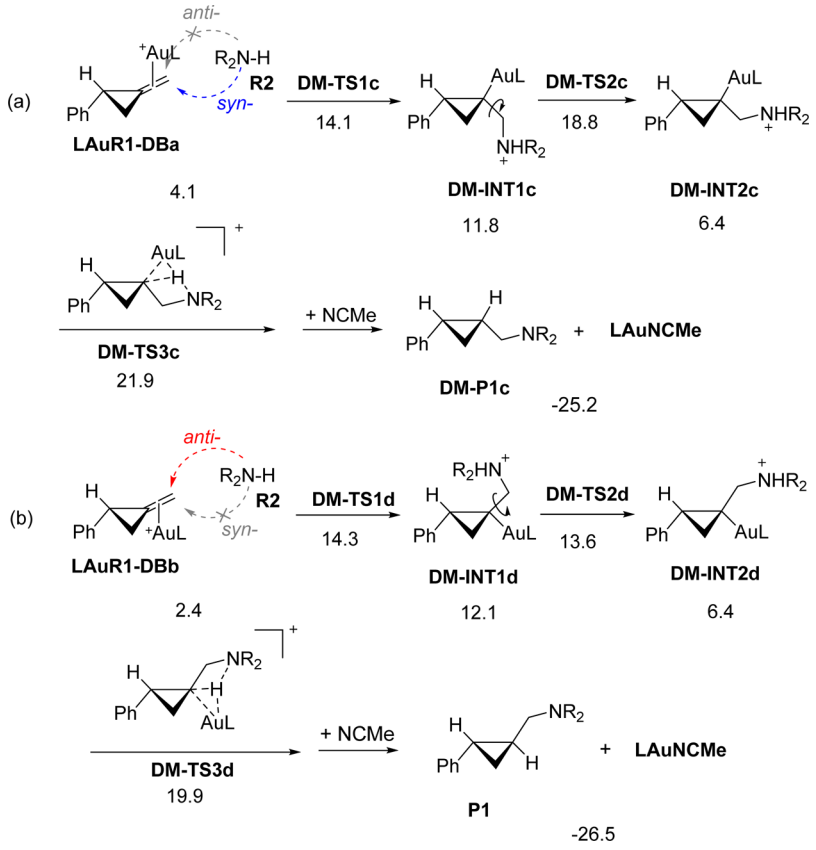

[a]Enthalpies are in kcal/mol.

Scheme 9. Possible Pathways for the Three-Membered-Ring Activation-First Mechanism[a]

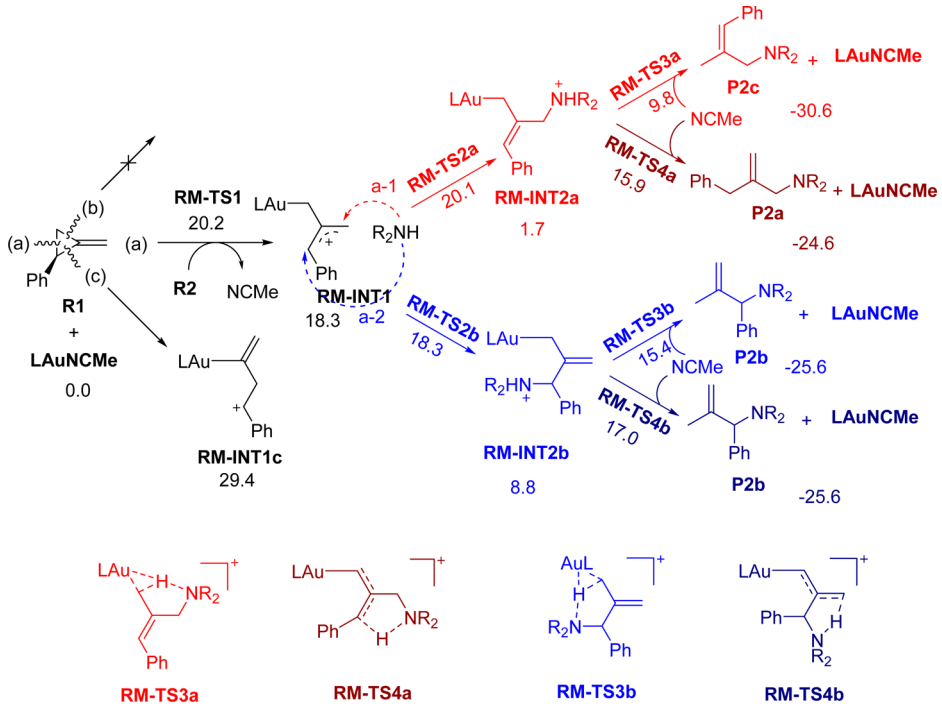

[a]Enthalpies are in kcal/mol.

TS4a. The relative enthalpies of **DM-TS3a** and **DM-TS4a** are 14.7 and 23.0 kcal/mol, respectively.

Starting from **LAuR1-DBb**, the *syn*- and *anti*- attack of **R2** to **R1** (Scheme 7) results in the formation of **DM-INT2a** and

DOI: 10.1021/acs.joc.6b00726
J. Org. Chem. 2016, 81, 7326−7335

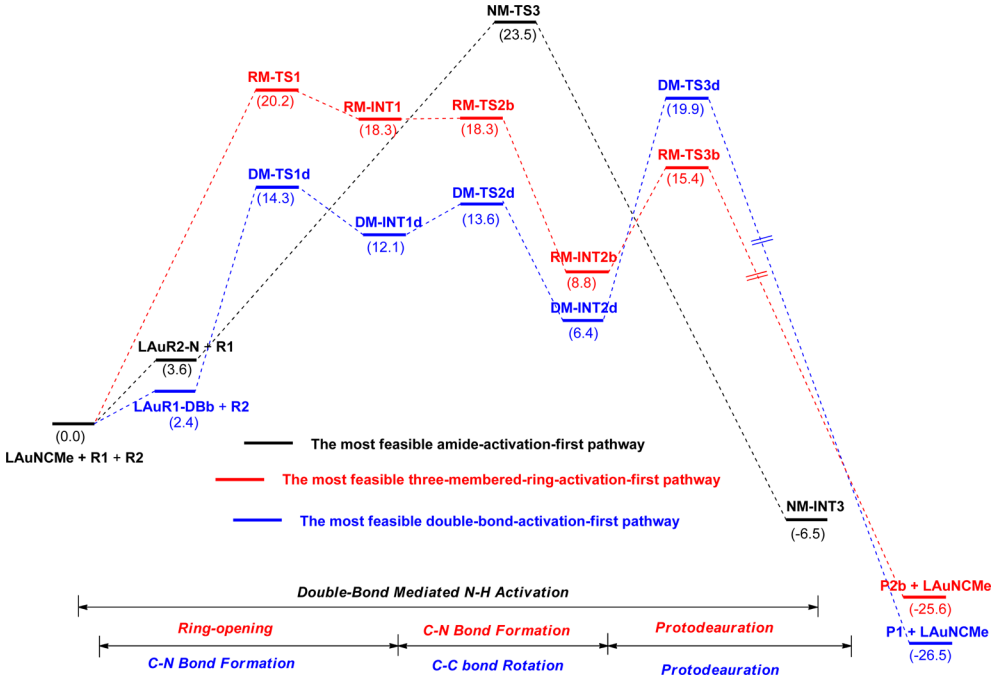

Figure 2. Comparison of the enthalpy profiles amide activation-first, double-bond activation-first, and three-membered-ring activation-first mechanisms.

DM-INT2b, respectively. The subsequent transformations of **DM-INT2a** or **DM-INT2b** will be the same as those in Scheme 6.

Furthermore, referring to the recent study on the Au(I)-catalyzed hydroamination of alkenes reported by Ujaque et al.,[7a] we also considered the mechanism involving hexafluoroantimonate anion-assisted proton transfer from the N atom to the carbonyl O atom. The enthalpy barrier of this proton transfer process is high (>30 kcal/mol), probably due to the weak basicity of hexafluoroantimonate anion. Therefore, the possibility for this mechanism has been excluded in our reaction system (see the Supporting Information for details).

According to the aforementioned results, the *syn*-product of the Markovnikov addition should proceed through the process **DM-TS1a** → **DM-INT1a** → **DM-TS3a** → **DM-INT2a** → **DM-TS4a** → **DM-P1a**, and the overall activation enthalpy is 23.0 kcal/mol (Scheme 6a and c). The *anti*-product of the Markovnikov addition proceeds through the process **DM-TS3b** → **DM-INT2b** → **DM-TS4b** → **DM-INT1b** → **DM-TS2b** → **DM-P1b**, and has an overall activation enthalpy of 20.1 kcal/mol (Schemes 7b and 6b, respectively). Herein, the *anti*-Markovnikov addition is relatively more favorable than the Markovnikov addition mechanism.

Different from the above Markovnikov hydroamination processes, N atom nucleophilically attacks the terminal carbon in *anti*-Markovnikov hydroamination. In principle, both *syn*- and *anti*-attack (*syn* and *anti* refer to the position of the phenyl and amine groups) might be plausible, whereas the *anti*-attack on **LAuR1-DBa** and *syn*-attack on **LAuR1-DBb** are disfavored. The reason might relate to the repulsion between **R2** and Au(I)L, and thus Au(I) easily approaches the three-membered ring and results in the automatic ring-opening (see the Supporting Information for details). In this context, only the *syn*-attack transition state on **LAuR1-DBa** and *anti*-attack transition state on **LAuR1-DBb** (**DM-TS1c** in Scheme 8a and DM-**TS1d** in Scheme 8b) can be located. After this step, the formed ammonium intermediates (**DM-INT1c** and **DM-INT1d**) easily isomerize to the more stable conformers (**DM-INT2c** and **DM-INT2d**) through the rotation of the C1−C2 bond and then undergo the protodeauration process to form the *anti*-Markovnikov products. As shown in Scheme 8, the **LAuR1-DBa** finally produces the *syn*-product of the *anti*-Markovnikov product (**DM-P1c**), while **LAuR1-DBb** finally produces the *anti*-Markovnikov product with an *anti*-configuration (**P1**). In these two pathways, the protodeauration steps are rate-determining, and the activation enthalpies are 21.9 and 19.9 kcal/mol, respectively.

Three-Membered-Ring Activation-First Mechanism. In principle, all three C−C bonds of the three-membered-ring in **R1** might undergo the bond dissociation process to give the ring-opened products. However, the calculation results show that the cleavage of the sp^3C-sp^3C bond is easier than that of the other two sp^2C-sp^3C bonds (Scheme 9 and Scheme S6). In Scheme 9, the sp^3C-sp^3C bond dissociation occurs with an activation enthalpy of 20.2 kcal/mol and generates the carbocation intermediate (**RM-INT1**) as the product. Then, the N atom of **R2** can attack the terminal carbon or the benzylic carbon of **RM-INT1**. The attack on the terminal carbon via **RM-TS2a** forms an ammonium intermediate (**RM-INT2a**), while the attack on the benzylic carbon via **RM-TS2b** forms **RM-INT2b** (Scheme 9). The enthalpies of **RM-TS2a** and **RM-TS2b** are 20.1 and 18.3 kcal/mol, respectively. Starting from **RM-INT2a**, the proton on the N atom can transfer to either the carbon connecting with the gold atom (i.e., protodeauration, **RM-INT2a** → **RM-TS3a** → **P2c**) or the benzylic carbon (**RM-INT2a** → **RM-TS4a** → **P2a**). The relative enthalpies of **RM-TS3a** and **RM-TS4a** are 9.8 and 15.9 kcal/mol, respectively.

Similar to **RM-INT2a**, **RM-INT2b** can also undergo two different proton-transfer processes to generate the final product (Scheme 9). The protodeauration occurs via transition state **RM-TS3b**, while the transfer of the proton to the terminal

DOI: 10.1021/acs.joc.6b00726
J. Org. Chem. 2016, 81, 7326−7335

carbon atom occurs via transition state **RM-TS4b**. Both proton-transfer processes finally generate the product **P2b**.

According to the calculation results in Scheme 9, the formation of different allylic amines undergo the same ring-opening step (**LAuNCMe + R1 → RM-TS1**), and this step is the rate-determining step of the ring-opening-first mechanisms. Thereafter, the different modes of the subsequent nucleophilic attack determine the configuration of the different products.

DISCUSSION

Comparison of Different Mechanisms. For a better view, the enthalpy profiles for the most favorable amide activation-first, double-bond activation-first, and three-membered-ring activation-first mechanisms are given in Figure 2. From Figure 2, the activation enthalpies for the rate-determining transition states in these three pathways are 23.5 (amide activation-first pathway: **NM-TS3** in Scheme 5), 19.9 (double-bond activation-first pathway: **DM-TS3d** in Scheme 8), and 20.2 kcal/mol (three-membered-ring activation-first pathway: **RM-TS1** in Scheme 9), respectively. The amide activation-first mechanism is excluded due to the relatively higher activation enthalpy. Meanwhile, the overall activation barrier of the double-bond activation-first is slightly lower than that of the three-membered-ring activation-first mechanism, indicating that the yield of the alkene hydroamination product should be more than (or at least comparable to) that of the three-membered ring opened product.[18] Herein, the theoretical conclusions are consistent with Widenhoefer's recent experiment that the predominant products were **P1** and **P2** (the ratio is 1.5:1, Scheme 2), while no C−O coupling product was generated.[5] On the basis of these two mechanisms, we finally provide some insights into the origin of the chemo-, regio-, and diastereoselectivity. In addition, the intermolecular hydroamination of several other substrates (including monoalkyl, dialkyl and dielectron-withdrawing-group substituted alkylidenecyclopropanes) has also been examined. Similar to our model reaction, the *anti*-products of the *anti*-Markovnikov hydroamination are the main products for all these systems. Meanwhile, for the alkyl and electron-withdrawing-group substituted ACPs, the ring-opened products are relatively depressed compared to that in the modeling reaction system (see the Supporting Information for more detailed results and discussion).

Chemoselectivity: Double-Bond Hydroamination vs Three-Membered Ring-Opening Products. Despite the overall activation barriers, the double-bond activation-first and three-membered-ring activation-first mechanisms are comparable (**DM-TS3d** in Scheme 8: 19.9 kcal/mol vs **RM-TS1** in Scheme 9: 20.2 kcal/mol), the rate-determining steps in these two mechanisms are distinct. For the double-bond activation-first mechanism, the final protodeauration is the rate-determining step. By contrast, the first step (i.e., the three-member ring opening step) is the rate-determining step of the three-membered-ring activation-first mechanism. Compared to the double-bond activation-first mechanism, the activation enthalpy of the protodeauration elementary step in the three-membered-ring activation-first mechanism is significantly lower (**RM-INT2b → RM-TS3d** in Scheme 9: 6.6 kcal/mol vs **DM-INT2d → DM-TS3d** in Scheme 8: 13.5 kcal/mol). As the ring-opening process results in the cationic intermediate **RM-INT1** (Scheme 9), the alkyl or electron-withdrawing-group substituents on the three-membered ring (instead of the aromatic ones) will destabilize the ring-opened product and the related transition state. Therefore, it is understandable that the ratio of the alkene hydroamination product could be significantly improved by replacing the aromatic group with alkyl groups in Widenhoefer's experiments.[5] Meanwhile, introducing electron-donating groups on the double bond/benzene groups might possibly facilitate the ring-opening of the alkylidenecyclopropane and thus benefit the formation of the ring-opened products.

To verify these predictions, the intermolecular hydroamination of several other substrates (including monoalkyl, dialkyl and dielectron-withdrawing-group substituted alkylidenecyclopropanes) was also calculated, and the results are given in Table 1. These calculation results imply that the *anti*-

Table 1. Calculations for the Gold-Catalyzed Intermolecular Hydroamination of Several Substituent Alkylidenecyclopropanes

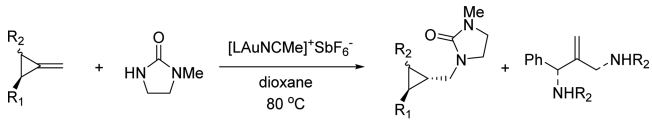

R1 R2 P1 P2

R1	$\Delta H^{\ddagger}_{\text{RM-TS1}}$	$\Delta H^{\ddagger}_{\text{DM-TS2b}}$ [b]	$\Delta H^{\ddagger}_{\text{DM-TS4d}}$ [c]	$\Delta H^{\ddagger}_{\text{DM-TS4c}}$ [d]	P1/P2
	20.2	20.1	19.9	21.9	1.5:1
 R1b	> 27.3[a]	21.2	22.5	22.7	≥ 25:1
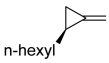 R1c	> 26.8[a]	20.8	22.3	22.1	≥ 25:1
 R1d	> 33.6[a]	19.6	23.0	22.7	≥ 25:1
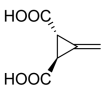 R1e	> 28.9[a]	18.8	22.3	/	≥ 25:1

[a]Enthalpies of the ring-opened intermediates (Enthalpies are in kcal/mol). [b]Leading to Markovnikov hydroamination products. [c]Leading to *anti*-Markovnikov hydroamination *anti*-products. [d]Leading to *anti*-Markovnikov hydroamination *syn*-products.

products of the *anti*-Markovnikov hydroamination are the most favorable products in different reaction systems. In addition, the high enthalpies of the ring-opened intermediates for these substituted alkylidenecyclopropanes (compared with that for the phenyl substituted one) could be attributed to the stabilizing effect of the phenyl substituent (rather than the alkyl or the electron-withdrawing substituents) on the cationic intermediate. The aforementioned results are consistent with the experimental observations: (1) *anti*-products of the *anti*-Markovnikov hydroamination are main products. (2) The ratio of the hydroamination products vs ring-opened products for

DOI: 10.1021/acs.joc.6b00726
J. Org. Chem. 2016, 81, 7326−7335

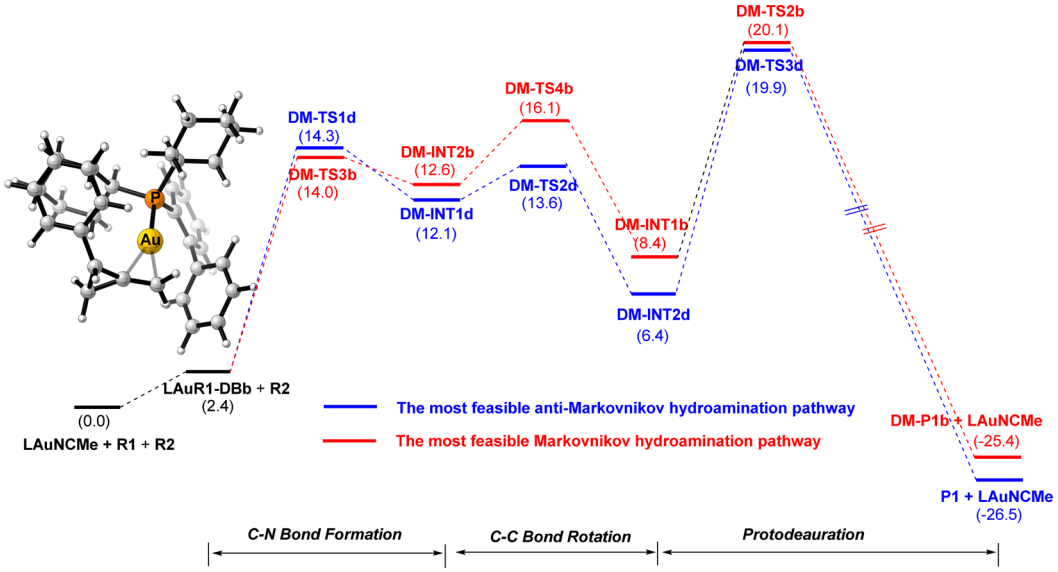

Figure 3. Comparison of the Markovnikov hydroamination and *anti*-Markovnikov hydroamination pathways.

Scheme 10. Distortion/Interaction Energy Analysis of DM-TS2c and DM-TS 2d[a]

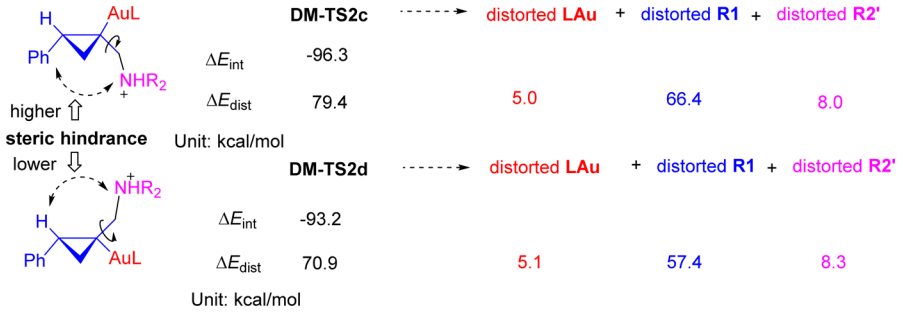

[a]The distorsion energies (ΔE_{dist}) are the electronic energy difference between the distorted segments (**LAu**, **R1**, and **R2**) and the optimized segments (**LAu**, **R1**, and **R2**). The interaction energies are the electronic energy difference between **DM-TS2c**/**DM-TS2d** and the distorted segments (**LAu**, **R1**, and **R2**)

the substituted alkylidenecyclopropanes is significantly higher than that for the modeling reactants (≥25:1 vs 1.5:1).

Regioselectivity: Markovnikov Hydroamination vs *Anti*-Markovnikov Hydroamination. Starting from the nucleophilic attack step (of the N atom of **R2** on the double bond of **R1**), the Markovnikov and *anti*-Markovnikov mechanisms become totally different. The attack of the N atom on the internal carbon finally leads to the Markovnikov product (Schemes 6 and 7), and the attack on the terminal carbon finally leads to the *anti*-Markovnikov product (Scheme 8). According to the calculation results (Figure 3), the two processes are competitive because the enthalpy demands of them are very close (**DM-TS3b** in Scheme 7: 14.0 kcal/mol vs **DM-TS1d** in Scheme 8: 14.3 kcal/mol). Therefore, the C−N bond formation step is not responsible for the regioselectivity. Besides, the relative enthalpies of the transition states in the rate-determining steps (**DM-TS2b** in Scheme 6: 20.1 kcal/mol vs **DM-TS3d** in Scheme 8: 19.9 kcal/mol) are also quite close in these two pathways. Therefore, the protodeautorotation is not responsible for the regioselectivity, either. In these two pathways, the most remarkable difference lies in the C1−C2 bond rotation step. In Markovnikov and *anti*-Markovnikov pathways, the enthalpy demands are 16.1 (**DM-TS4b** in Scheme 7) and 13.6 kcal/mol (**DM-TS2d** in Scheme 8), respectively. The results indicate that the latter mechanism occurs ca. 70 times faster than the former one. In addition, the formed ammonium intermediate (precursor of the rate-determining protodeauration step) in the Markovnikov pathway is less stable than that in the *anti*-Markovnikov pathway (**DM-INT1b** in Scheme 6: 8.4 kcal/mol vs **DM-INT2d** in Scheme 8: 6.4 kcal/mol). Therefore, the relative facility for formation of the *anti*-Markovnikov ammonium intermediate determines the regioselectivity from both kinetic and thermodynamic aspects.

Diastereoselectivity: *Syn*-Product vs *Anti*-Product. In *anti*-Markovnikov double-bond hydroamination pathways (Scheme 8), the nucleophilic attack is sensitive to the steric effect. Therefore, the chirality of the C2 atom in the product is directly determined by the initial configuration of the double-bond-coordinated intermediate **LAuR1-DBa** and **LAuR1-DBb** (Scheme 3). In **LAuR1-DBa**, Au(I)L is *anti* to the phenyl group and the *syn* nucleophic attack finally generates the *syn*-product (Scheme 8a). In **LAuR1-DBb**, the gold atom is *syn* to the phenyl group, and the *anti*-product is finally formed after the *anti*-attack (Scheme 8b). Both pathways proceed through three steps: C−N bond formation, C1−C2 bond rotation, and protodeauration. Among these steps, the C−N bond formation steps require similar enthalpy demands for these two pathways

DOI: 10.1021/acs.joc.6b00726
J. Org. Chem. 2016, 81, 7326−7335

(**DM-TS1c** in Scheme 8a: 14.1 kcal/mol for the *syn*-product vs **DM-TS1d** in Scheme 8b: 14.3 kcal/mol for the *anti*-product). By contrast, the C1−C2 rotation step for the *anti*-product is much more facile than that for the *syn*-product (**DM-TS2d** in Scheme 8b: 13.6 kcal/mol vs **DM-TS2c** in Scheme 8a: 18.8 kcal/mol). Meanwhile, the subsequent protodeauration step for the *anti*-product is also easier than that for the *syn*-product (**DM-TS3d** in Scheme 8b: 19.9 kcal/mol vs **DM-TS3c** in Scheme 8a: 21.9 kcal/mol). These results suggest that both the C1−C2 rotation and the protodeauration steps contribute to the diastereoselectivity. In other words, the relatively rapid formation and decomposition of the ammonium intermediate in the *anti*-pathway results in the diastereoselectivity. The reason for these results has been analyzed by the distortion/interaction model developed by Houk et al.[19] Herein the two key transition states involved in the C1−C2 rotation steps (**DM-TS2c** in Scheme 8a: 18.8 kcal/mol and **DM-TS2d** in Scheme 8b: 13.6 kcal/mol) are used for discussions, and the discussions on the transition states involved in the protodeauration step (**DM-TS3c** in Scheme 8a: 21.9 kcal/mol vs **DM-TS3d** in Scheme 8b: 19.9 kcal/mol) are given in the Supporting Information (Scheme S7). According to the distortion/interaction model, either **DM-TS2c** or **DM-TS2d** could be separated into three segments: distorted **LAu**, distorted **R1**, and distorted **R2**. The results in Scheme 10 show that the interaction energy of **DM-TS2c** is lower than that of **DM-TS2d** by 3.1 kcal/mol, whereas the distortion energy of **DM-TS2c** is much higher than that of **DM-TS2d** by 8.5 kcal/mol. The significant distortion energy difference is dominantly caused by the **R1** segments. Therefore, the reactivity for the C1−C2 rotation step is controlled by the distortion energy, especially by the distortion energy of the **R1** segment. The relatively lower steric hindrance in rotating the NHR_2^+ group in **DM-INT1d** (than that in **DM-INT1c**) might benefit the stability of the skeleton structure of the **R1** moiety and thus results in the lower distortion energy therein.

CONCLUSION

In this study, the mechanism of the gold-catalyzed intermolecular hydroamination of alkylidenecyclopropane with 1-methylimidazolidin-2-one was theoretically investigated. It is found that the double-bond activation-first and the three-membered-ring activation-first mechanisms might be competitive in the reaction system. The double-bond activation-first mechanism proceeds through three steps: C−N bond formation, C1−C2 rotation, and protodeauration. The protodeauration is the rate-determining step. The three-membered ring-first mechanism occurs through the ring-opening, C−N bond formation, and protodeauration steps. The ring-opening step is the rate-determining step. The aromatic substituent on the three-membered ring might stabilize the key cationic intermediates and transition states and thus facilitates the formation of the ring-opened product (with decreased ratio of alkene hydroamination product). The regioselectivity (i.e., Markovnikov hydroamination vs *anti*-Markovnikov hydroamination) is determined by the C−C bond (the alkene bond in the substrate) rotation step and the diastereoselectivity is related to both the C−C bond rotation and the protodeauration steps. The calculation results are in good agreement with the experimental observations on the obtained chemo-, regio-, and stereoselectivity. These results are expected to provide valuable information for the future development of new strategies in gold-catalyzed reactions.

ASSOCIATED CONTENT

Supporting Information

The Supporting Information is available free of charge on the ACS Publications website at DOI: 10.1021/acs.joc.6b00726.

Direct oxidative addition of the N−H bond of **R2** to Au(I), external base-assisted activation of N−H bond, ACP-mediated N−H activation mechanism starting from **LAuR2-O**, *anti*-attack transition state on **LAuR1-DBa** and *syn*-attack transition state on **LAuR1-DBb**, hexafluoroantimonate anion-assisted proton-transfer process, cleavage of the three bonds of the three-membered ring of **R1**, distortion/interaction energy analysis of **DM-TS3c** and **DM-TS3d**, comparison of the enthalpies, zero-point vibration energy corrected energies, Gibbs free energies and B3LYP-D3BJ-enthalpies, Cartesian coordinates, and energy properties of reactants, intermediates, and transition states (PDF)

AUTHOR INFORMATION

Corresponding Authors

*E-mail: qichenze@usx.edu.cn.

*E-mail: yuhaizhu@ahu.edu.cn.

Notes

The authors declare no competing financial interest.

ACKNOWLEDGMENTS

We thank the NSFC (No. 21202102) for financial support and scientific research funds from Anhui University (J01006021). All calculations in this study were performed at the Supercomputer Center of Shenzhen.

REFERENCES

(1) (a) Dorel, R.; Echavarren, A. M. *Chem. Rev.* **2015**, *115*, 9028−9072. (b) Zeng, X. *Chem. Rev.* **2013**, *113*, 6864−6900. (c) Corma, A.; Leyva-Pérez, A.; Sabater, M. J. *Chem. Rev.* **2011**, *111*, 1657−1712. (d) Patil, N. T.; Kavthe, R. D.; Shinde, V. S. *Tetrahedron* **2012**, *68*, 8079−8146. (e) Huang, X.; Klimczyk, S.; Veiros, L. F.; Maulide, N. *Chem. Sci.* **2013**, *4*, 1105−1110. (f) Klimczyk, S.; Misale, A.; Huang, X.; Maulide, N. *Angew. Chem., Int. Ed.* **2015**, *54*, 10365−10369. (g) Zhu, S. F.; Hu, L.; Jiang, H. F. *Org. Biomol. Chem.* **2014**, *12*, 4104−4111.

(2) (a) Huang, L.; Arndt, M.; Gooßen, K.; Heydt, H.; Gooßen, L. *Chem. Rev.* **2015**, *115*, 2596−2697. (b) Müller, T. E.; Hultzsch, K. C.; Yus, M.; Foubelo, F.; Tada, M. *Chem. Rev.* **2008**, *108*, 3795−3892. (c) Li, J.; Wang, H.; Sun, J.; Yang, Y.; Liu, L. *Org. Biomol. Chem.* **2014**, *12*, 2523−2527. (d) Lo, V. K. Y.; Chan, A. O. Y.; Che, C. M. *Org. Biomol. Chem.* **2015**, *13*, 6667−6680.

(3) For selected examples of transition-metal-catalyzed Markovnikov hydroamination of alkenes, see: (a) Ickes, A. R.; Ensign, S. C.; Gupta, A. K.; Hull, K. L. *J. Am. Chem. Soc.* **2014**, *136*, 11256−11259. (b) Sevov, C. S.; Zhou, J.; Hartwig, J. F. *J. Am. Chem. Soc.* **2014**, *136*, 3200−3207. (c) Zhang, Z.; Lee, S. D.; Widenhoefer, R. A. *J. Am. Chem. Soc.* **2009**, *131*, 5372−5373. (d) LaLonde, R. L.; Brenzovich, W. E., Jr.; Benitez, D.; Tkatchouk, E.; Kelley, K.; Goddard, W. A., III; Toste, F. D. *Chem. Sci.* **2010**, *1*, 226−233.

(4) For selected examples of transition-metal-catalyzed *anti*-Markovnikov hydroamination of alkenes, see: (a) Utsunomiya, M.; Kuwano, R.; Kawatsura, M.; Hartwig, J. F. *J. Am. Chem. Soc.* **2003**, *125*, 5608−5609. (b) Takaya, J.; Hartwig, J. F. *J. Am. Chem. Soc.* **2005**, *127*, 5756−5757. (c) Rucker, R. P.; Whittaker, A. M.; Dang, H.; Lalic, G. *J. Am. Chem. Soc.* **2012**, *134*, 6571−6574. (d) Bronner, S. M.; Grubbs, R. H. *Chem. Sci.* **2014**, *5*, 101−106.

(5) Timmerman, J. C.; Robertson, B. D.; Widenhoefer, R. A. *Angew. Chem., Int. Ed.* **2015**, *54*, 2251−2254.

DOI: 10.1021/acs.joc.6b00726
J. Org. Chem. 2016, 81, 7326−7335

(6) (a) Zhang, D.-H.; Du, K.; Shi, M. *Org. Biomol. Chem.* **2012**, *10*, 3763−3766. (b) Nakamura, I.; Itagaki, H.; Yamamoto, Y. *J. Org. Chem.* **1998**, *63*, 6458−6459. (c) Siriwardana, A. I.; Kamada, M.; Nakamura, I.; Yamamoto, Y. *J. Org. Chem.* **2005**, *70*, 5932−5937. (d) Shi, M.; Liu, L.-P.; Tang, J. *Org. Lett.* **2006**, *8*, 4043−4046. (e) Liu, R. R.; Ye, S. C.; Lu, C. J.; Xiang, B.; Gao, J. R.; Jia, Y. X. *Org. Biomol. Chem.* **2015**, *13*, 4855−4858.

(7) (a) Hase, S.; Kayaki, Y.; Ikariya, T. *ACS Catal.* **2015**, *5*, 5135−5140. (b) Yuan, R.; Lin, Z. *ACS Catal.* **2015**, *5*, 2866−2872. (c) Couce-Rios, A.; Kovács, G.; Ujaque, G.; Lledós, A. *ACS Catal.* **2015**, *5*, 815−829. (d) Ciancaleoni, G.; Belpassi, L.; Zuccaccia, D.; Tarantelli, F.; Belanzoni, P. *ACS Catal.* **2015**, *5*, 803−814. (e) Ariafard, A. *ACS Catal.* **2014**, *4*, 2896−2907. (f) Ariafard, A. *ACS Catal.* **2014**, *4*, 2896−2907. (g) Zhou, Q.; Li, Y. *J. Am. Chem. Soc.* **2014**, *136*, 1505−1513.

(8) (a) Kovács, G.; Ujaque, G.; Lledós, A. *J. Am. Chem. Soc.* **2008**, *130*, 853−864. (b) Fang, R.; Wei, X. X.; Yang, L. Z. *Org. Biomol. Chem.* **2014**, *12*, 8433−8441.

(9) Jiang, M.; Liu, L.-P.; Shi, M.; Li, Y. *Org. Lett.* **2010**, *12*, 116−119.

(10) Frisch, M. J.; Trucks, G. W.; Schlegel, H. B.; Scuseria, G. E.; Robb, M. A.; Cheeseman, J. R.; Scalmani, G.; Barone, V.; Mennucci, B.; Petersson, G. A.; Nakatsuji, H.; Caricato, M.; Li, X.; Hratchian, H. P.; Izmaylov, A. F.; Bloino, J.; Zheng, G.; Sonnenberg, J. L.; Hada, M.; Ehara, M.; Toyota, K.; Fukuda, R.; Hasegawa, J.; Ishida, M.; Nakajima, T.; Honda, Y.; Kitao, O.; Nakai, H.; Vreven, T.; Montgomery, J. A., Jr.; Peralta, J. E.; Ogliaro, F.; Bearpark, M.; Heyd, J. J.; Brothers, E.; Kudin, K. N.; Staroverov, V. N.; Kobayashi, R.; Normand, J.; Raghavachari, K.; Rendell, A.; Burant, J. C.; Iyengar, S. S.; Tomasi, J.; Cossi, M.; Rega, N.; Millam, N. J.; Klene, M.; Knox, J. E.; Cross, J. B.; Bakken, V.; Adamo, C.; Jaramillo, J.; Gomperts, R.; Stratmann, R. E.; Yazyev, O.; Austin, A. J.; Cammi, R.; Pomelli, C.; Ochterski, J. W.; Martin, R. L.; Morokuma, K.; Zakrzewski, V. G.; Voth, G. A.; Salvador, P.; Dannenberg, J. J.; Dapprich, S.; Daniels, A. D.; Farkas, Ö.; Foresman, J. B.; Ortiz, J. V.; Cioslowski, J.; Fox, D. J. *Gaussian 09*, Revision D.01; Gaussian, Inc.: Wallingford, CT, 2009.

(11) (a) Becke, A. D. *Phys. Rev. A: At., Mol., Opt. Phys.* **1988**, *38*, 3098−3100. (b) Lee, C.; Yang, W.; Parr, R. G. *Phys. Rev. B: Condens. Matter Mater. Phys.* **1988**, *37*, 785−789.

(12) Marenich, A. V.; Cramer, C. J.; Truhlar, D. G. *J. Phys. Chem. B* **2009**, *113*, 6378−6396.

(13) Fukui, K. *Acc. Chem. Res.* **1981**, *14*, 363−368.

(14) (a) Zhao, Y.; Truhlar, D. G. *J. Phys. Chem. A* **2006**, *110*, 13126−13130. (b) Zhao, Y.; Truhlar, D. G. *Acc. Chem. Res.* **2008**, *41*, 157−167. (c) Zhao, Y.; Truhlar, D. G. *Chem. Phys. Lett.* **2011**, *502*, 1−13.

(15) The Gibbs free energies are given in the Supporting Information (Table S2). Based on the Eyring equation, the overall activation barrier is roughly estimated to be 28 kcal/mol according to Widenhoefer's experimental outcome (80 °C, 18h, 99% conversion). This data is significantly lower than the activation Gibbs free energy (43.2 kcal/mol, corresponding to transition state DM-TS3d in Scheme 9), confirming that the entropic effect is overestimated.

(16) (a) Sakaki, S.; Takayama, T.; Sumimoto, M.; Sugimoto, M. *J. Am. Chem. Soc.* **2004**, *126*, 3332−3348. (b) Tamura, H.; Yamazaki, H.; Sato, H.; Sakaki, S. *J. Am. Chem. Soc.* **2003**, *125*, 16114−16126. (c) Li, H.; Zhao, L.; Lu, G.; Mo, Y.; Wang, Z.-X. *Phys. Chem. Chem. Phys.* **2010**, *12*, 5268−5275. (d) Marcelli, T. *Angew. Chem., Int. Ed.* **2010**, *49*, 6840−6843. (e) Yang, Z.-D.; Pal, R.; Hoang, G. L.; Zeng, X.-C.; Takacs, J. M. *ACS Catal.* **2014**, *4*, 763−773. (f) Plata, R. E.; Singleton, D. A. *J. Am. Chem. Soc.* **2015**, *137*, 3811−3826. (g) Wu, J.-C.; Xu, W.-B.; Yu, Z.-X.; Wang, J. *J. Am. Chem. Soc.* **2015**, *137*, 9489−9496.

(17) Comas-Vives, A.; Ujaque, G. *J. Am. Chem. Soc.* **2013**, *135*, 1295−1305.

(18) Despite that the differences below 1−2 kcal/mol are below the error bar of quantum chemical methods, the relative facilities of different pathways could be reliable due to the systematic overestimation or underestimation.

(19) (a) Ess, D. H.; Houk, K. N. *J. Am. Chem. Soc.* **2007**, *129*, 10646−10647. (b) Ess, D. H.; Houk, K. N. *J. Am. Chem. Soc.* **2008**, *130*, 10187−10198. (c) Paton, R. S.; Kim, S.; Ross, A. G.; Danishefsky, S. J.; Houk, K. N. *Angew. Chem., Int. Ed.* **2011**, *50*, 10366−10368. (d) Liu, F.; Paton, R. S.; Kim, S.; Liang, Y.; Houk, K. N. *J. Am. Chem. Soc.* **2013**, *135*, 15642−15649.

DOI: 10.1021/acs.joc.6b00726
J. Org. Chem. 2016, 81, 7326−7335